Editors' Suggestion

Particulate Projectiles Driven by Cavitation Bubbles

Zibo Ren, Zhigang Zuo,* Shengji Wu, and Shuhong Liu†
State Key Laboratory of Hydroscience and Engineering, and Department of Energy and Power Engineering, Tsinghua University, 100084 Beijing, China

(Received 5 September 2021; revised 14 November 2021; accepted 15 December 2021; published 26 January 2022)

The removal of surface-attached particles with cavitation bubbles is usually attributed to the jetting or shear stresses when bubbles collapse. In this Letter, we report an unexpected phenomenon that millimeter-sized spherical particles made of heavy metals (e.g., stainless steel), when initially resting on a fixed rigid substrate, are suddenly accelerated like projectiles through the production of nearby laser-induced cavitation bubbles of similar sizes. We show experimentally and theoretically that the motion of a particle with radius R_p is determined by the maximum bubble radius $R_{b,\max}$, the initial distance from the laser focus to the center of the particle L_0, and the initial azimuth angle φ_0. We identify two dominant regimes for the particle's sudden acceleration, namely, the unsteady liquid inertia dominated regime and the bubble contact dominated regime, determined by $R_{b,\max}R_p/L_0^2$. We find the nondimensional maximum vertical displacement of the particle follows the fourth power and the square power scaling laws for respective regimes, which is consistent with the experimental results. Our findings can be applied to nonintrusive particle manipulation from solid substrates in a liquid.

DOI: 10.1103/PhysRevLett.128.044501

Cavitation in a liquid containing particles exists in various technological fields, e.g., cavitation erosion of hydraulic machinery in silt-laden rivers [1,2], ultrasonic cleaning [3], kidney stone fragmentation [4], etc. These processes involve interactions of cavitation bubbles with free and/or surface-attached particles, being attributed to the collapsing cavitation bubbles, including microjetting toward boundaries, consequent complex flows [5,6] and shock wave emissions [7]. Upon generation, a cavitation bubble expands with a tremendous velocity, during which period the influences on a nearby particle have not been fully investigated.

Over the last two decades, a number of studies have indicated that the explosive growth of the cavitation bubbles accelerates the particles in an infinite liquid both on the millimeter [8,9] and on the micrometer scales [10–13]. In the vicinity of a rigid boundary, recent studies have focused on the impact of free-settling microparticles onto the solid boundary accelerated by millimeter-sized cavitation bubbles [14,15], presumably causing cavitation damage. Yet the role of growing cavitation bubbles in removing particles from surfaces has largely been neglected.

In this Letter, we report the unexpected phenomenon that a heavy surface-attached particle, interacting with a nearby cavitation bubble of similar size, is not only removed from the surface, but also accelerates like a projectile with a *controllable* vertical displacement. The reason for the particle's acceleration is revealed with theoretical analysis and scaling laws are proposed for the forces on the particle and the particle's trajectory determined by initial controllable parameters.

By using tweezers, a spherical particle (radius $R_p = 2.0$–3.0 mm) is placed onto the horizontal upper surface of a fixed plate (area 100 mm × 50 mm) in filtered, deionized, and degassed water (O_2 concentration 2.3–4.3 mg/l); see Fig. 1. The plate is made of stainless steel with a polished surface of an average roughness of 0.83 μm (Surface profiler, Zygo Nexview, U.S.A.) to lessen friction between the plate and a particle. A cavitation bubble with a maximum radius of $R_{b,\max} = 1.5$–3.0 mm (equivalent radius with the same bubble volume as a sphere) is induced in the vicinity of the particle by a focused Q-switched pulsed ruby laser (QSR9, Innolas Ltd., U.K.). The location of the laser focus is aligned to the plane of $y = 0$ with a high-speed camera (FASTCAM Mini UX50, Photron, Japan) monitoring from the top view. From the side view, the cavitation bubble and the particle are recorded with a high-speed camera (Phantom v711, Vision Research Inc., U.S.A.) with different maximum bubble

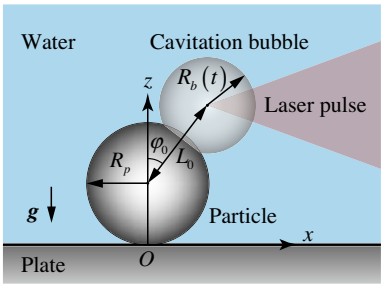

FIG. 1. Experimental configuration (side view) and notation.

radii $R_{b,\max}$, initial distances from the laser focus to the center of the particle L_0, and initial azimuth angles φ_0. The laser and the high-speed cameras are synchronously triggered by a delay generator (9524, Quantum Composers Inc., U.S.A.). Stainless steel particles of radii $R_p = 2.0$, 2.5, and 3.0 mm (density $\rho_p = 7.9 \times 10^3$ kg/m^3) and brass particles of radii $R_p = 2.5$ mm (density $\rho_p = 8.3 \times 10^3$ kg/m^3) are placed at the start of the experiments.

First we show the behaviors of a stainless steel particle ($R_p = 2.5$ mm) with different L_0, $R_{b,\max}$ and φ_0; see Fig. 2. For case A with $\varphi_0 \approx 0°$ and at a small distance $L_0 \approx 1.2R_p$ from a cavitation bubble with $R_{b,\max} \approx 0.8R_p$, the particle detaches from the substrate *before* the bubble reaches its maximum size at 0.203 ms; see the enlarged snapshot in Fig. 2(a). The particle continues its rise as the bubble collapses. After the bubble rebounds several times until it disappears, the particle travels vertically in the water with a maximum vertical displacement of $\approx 4.6R_p$. Finally, the particle returns and impacts on the substrate, where it bounces several times until it stops.

With similar L_0 and $R_{b,\max}$ and for larger initial azimuth angles of $\varphi_0 \approx 30°$ (case B) and $\varphi_0 \approx 60°$ (case C), the particle still detaches from the substrate during the bubble growth; see the enlarged snapshots at 0.215 ms in Fig. 2(b) and at 0.228 ms in Fig. 2(c). Subsequently, the particle makes an oblique projectile motion with smaller maximum vertical displacements compared with case A. To our surprise, even when the cavitation bubble is generated far away from the particle ($L_0 \approx 2.4R_p$, case D), the particle can still detach from the substrate. The detachment of the particle is hardly visualized during the bubble growth, this time with a maximum vertical displacement greatly reduced to $\approx 0.25R_p$ [Fig. 2(d)]. The particle's projectile motion is reasonably attributed to the initial velocity the particle achieves during its interaction with the cavitation bubble. Thus, we look into the particle motion during the bubble's growth and collapse.

To understand the quantitative mechanism of the particle's sudden acceleration, we adapt the theoretical model by Best and Blake [17] for a stationary rigid sphere near a cavitation bubble, where the flow field was given by the Weiss sphere theorem [18]. In our case, the plate is considered as a hydrodynamics mirror because the Reynolds number is sufficiently large [19], thus including the images of the particle and the bubble [panel (i) in Fig. 3(a)]. For simplicity, the dynamics of the cavitation bubble is approximated by the Rayleigh equation for spherical bubbles (with timescale $R_{b,\max}\sqrt{\rho/\Delta p}$ with $\Delta p = p_\infty - p_v$ and the vapor pressure p_v [2]), which fits well with the experimental results during the bubble growth [Fig. 3(b)]. Then, the velocity potential of the flow field around the particle $\Phi(x, y, z, t)$ is resolved by the superposition of basic solutions [16]. Thus, we use the unsteady Bernoulli equation, which reads

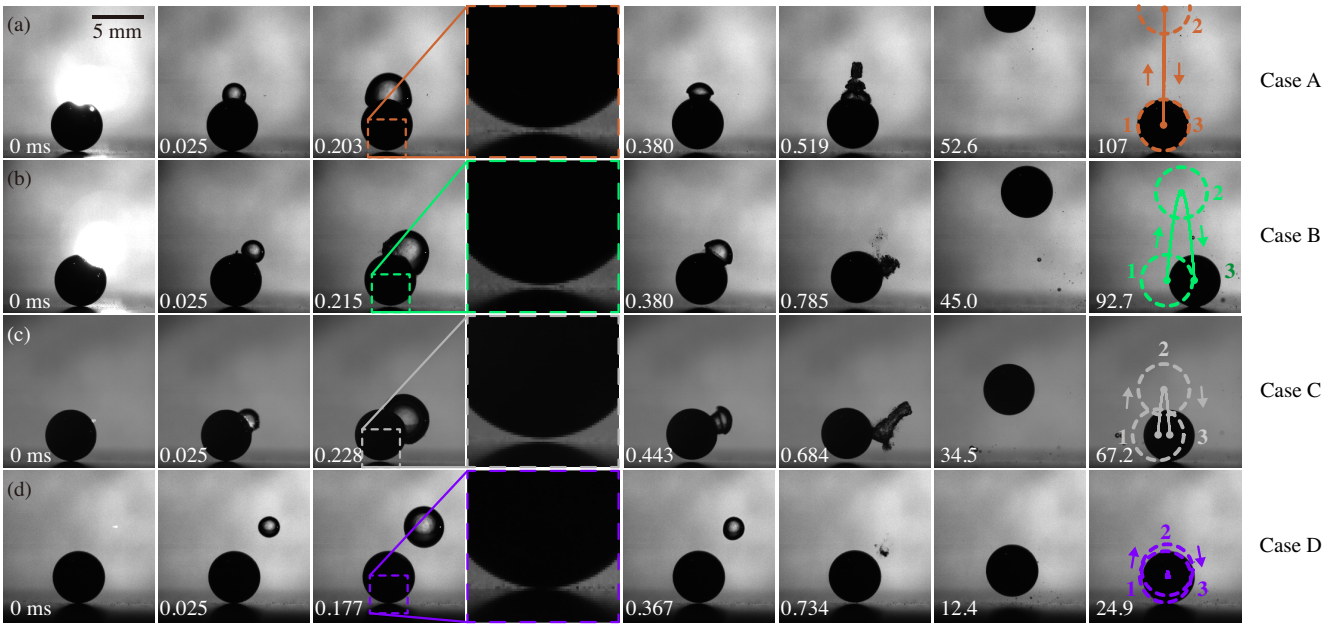

FIG. 2. Image sequences showing the sudden acceleration of a stainless steel particle (radius $R_p = 2.5$ mm) from a substrate made of stainless steel by cavitation bubbles for (a) case A, $\varphi_0 = 3.4°$, $L_0/R_p = 1.17$, $R_{b,\max}/R_p = 0.83$; (b) case B, $\varphi_0 = 31°$, $L_0/R_p = 1.20$, $R_{b,\max}/R_p = 0.84$; (c) case C, $\varphi_0 = 56°$, $L_0/R_p = 1.04$, $R_{b,\max}/R_p = 0.89$; and (d) case D, $\varphi_0 = 35°$, $L_0/R_p = 2.37$, $R_{b,\max}/R_p = 0.81$. The regions focused on the bottoms of the particles are enlarged in the fourth column. The last column displays the superimposition of the outlines of the particle at the initial position ("1"), at the maximum height ("2"), and the snapshot of impact of the fallen particle on the plate ("3"). The trajectory of the center of the particle in each case is visualized by the solid line. Videos are provided in the Supplemental Material [16].

$$p = p_\infty - \rho\frac{\partial\Phi}{\partial t} - \rho\frac{\|\nabla\Phi\|^2}{2} + \rho g(z_\infty - z), \qquad (1)$$

with the pressure in the far field p_∞, the density of water ρ, the gravitational acceleration g, and the baseline in the far field at $z_\infty = 0$ to resolve the pressure distribution *in the liquid*. Moreover, we consider the pressure on the particle equals the vapor pressure in the contact region of the cavitation bubble with the particle for $R_p + R_b > L_0$. The hydrodynamic forces exerted on the particle are subsequently calculated by numerical integration around the particle's surface.

Figures 3(c) and 3(d) show the evolution of the vertical and horizontal components of the hydrodynamic forces on the particle calculated for cases A–D. The vertical force converts from a compressive force to a lift force during the bubble growth highlighted by the yellow region. This conversion, with its highly time-dependent feature, can be understood by the leading contribution of the unsteady pressure around the particle, i.e., $p \sim -\rho(\partial\Phi/\partial t)$. The potential Φ is proportional to the volume growth rate of the bubble $Q(t) = 4\pi R_b^2\dot{R}_b$ with the radius R_b and the velocity of the bubble-liquid interface $\dot{R}_b$. Thus, the resultant force on the spherical particle $\boldsymbol{F} = \oiint -p d\boldsymbol{S}$ is approximately proportional to $(dQ/dt) = 4\pi(2R_b\dot{R}_b^2 + R_b^2\ddot{R}_b)$ with the acceleration of the bubble-liquid interface $\ddot{R}_b$. At $t \to 0$, the bubble expands at a tremendous speed $\dot{R}_b$, leading to large (dQ/dt). As a result, the resultant force presses the spherical particle on the rigid boundary in the vertical direction, while pushing the particle away from the bubble in the horizontal direction [panel (ii) in Fig. 3(a)]. The bubble then undergoes a decelerating expansion with $2R_b\dot{R}_b^2 > 0$ and $R_b^2\ddot{R}_b < 0$, and thus (dQ/dt) decreases to zero and changes its sign, inducing the conversion of the resultant force composed of a lift force in the vertical direction and an attractive force in the horizontal direction [panel (iii) in Fig. 3(a)].

Next, we verify that our theoretical model gives a reasonable prediction of the particle displacements during the bubble's growth and collapse. Since the translations of the particle by the end of the bubble's collapse are smaller than $0.05R_p$ in both vertical and horizontal directions [experimental data in Figs. 3(e) and 3(f)], a simple way to calculate the particle displacements is to adopt the evolution of the forces in Figs. 3(c) and 3(d), ignoring the influence of the small translations of the particle on the flow field. Since all the surface forces on the particle have been included in the component forces F_z and F_x, the force balance on the particle in the vertical direction reads $F_z - m_p g = m_p a_{p,z}$ with the mass of the particle m_p and the component acceleration $a_{p,z}$, and in the horizontal direction $F_x = m_p a_{p,x}$ with the component acceleration $a_{p,x}$. By time integral, the displacements of the particle are displayed in Figs. 3(e) and 3(f), both being quantitatively consistent with the experimental results. On a longer timescale, the rebounds of the bubbles may exert forces on the particle in similar manners discussed above, interfering more with the horizontal motion of the particle at smaller standoff distances to the plate (e.g., case C).

In our analysis, the contact of the bubble and the particle also contributes to a particle's sudden acceleration. To verify this experimentally, by the balance of momentum in

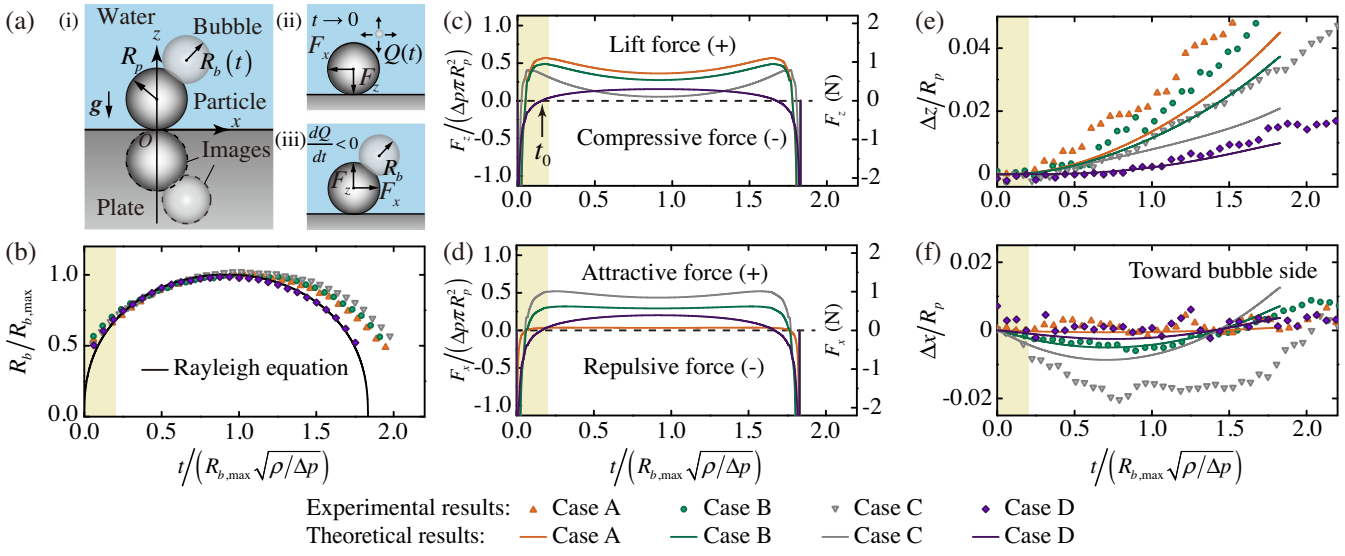

FIG. 3. Experimental and theoretical results for the particle's sudden acceleration. (a) Theoretical model. (i) Sketch of the method of images. Hydrodynamic forces on the particle (ii) at the bubble generation and (iii) when the bubble's volume growth rate $Q(t)$ slows down. (b) Evolution of the normalized bubble radius. The black line is based on the solution to the Rayleigh equation for a spherical bubble. The forces exerted on the particle are shown in the (c) vertical and (d) horizontal directions. The yellow areas highlight the time period of the force conversion. The normalized particle displacements are shown in the (e) vertical and (f) horizontal directions.

the vertical direction from the bubble's nucleation to its first collapse ΔT, the time-averaged component force $\langle F_z \rangle$ exerted on the particle can be estimated as $\langle F_z \rangle = m_p v_{0,z}/\Delta T$, with the initial vertical velocity $v_{0,z}$ estimated from the time average during the approximate uniform motion of the particle after detachment. Figure 4(a) displays the normalized force $\langle F_z \rangle^* = \langle F_z \rangle/(\Delta p \pi R_p^2 \cos\varphi_0)$ versus $R_{b,\max}R_p/L_0^2$, with experimental results of stainless steel and brass particles with $\varphi_0 \in (0°, 80°)$, $L_0/R_p \in (1.0, 3.6)$, and $R_{b,\max}/R_p \in (0.4, 1.2)$, leading to $R_{b,\max}R_p/L_0^2 \in (0.05, 1.1)$.

For cases without bubble-particle contact, the approximate linear relationship between $\langle F_z \rangle^*$ and $R_{b,\max}R_p/L_0^2$ [Fig. 4(a)] can be understood by the scaling of the hydrodynamic force from the unsteady liquid inertia, i.e., $\langle F_z \rangle \sim \langle \oiint \rho(\partial\Phi/\partial t)\boldsymbol{n}_z \cdot d\boldsymbol{S} \rangle = \rho\langle dQ/dt \rangle I(R_p, L_0, \varphi_0)$, with a surface integral independent of time $I(R_p, L_0, \varphi_0)$ with the dimension of length. The time-averaged (dQ/dt) from t_0 [when F_z changes its sign to positive, e.g., marked for case D in Fig. 3(c)] to ΔT (twice the Rayleigh collapse time) reads $\langle dQ/dt \rangle = \{[Q(\Delta T) - Q(t_0)]/\Delta T\}$; note $t_0 \ll \Delta T$. At $t = \Delta T$, the bubble shrinks to the minimum volume ($R_b \approx 0$), giving $Q(\Delta T) = 0$. Solving $(dQ/dt) = 0$ at $t = t_0$ with $\dot{R}_b = \sqrt{\frac{2}{3}(\Delta p/\rho)[(R_{b,\max}/R_b)^3 - 1]}$ [20], we approximate $Q(t_0)$ as $7.05R_{b,\max}^2\sqrt{(\Delta p/\rho)}$ and thus $\langle F_z \rangle$ as $-3.85\Delta p R_{b,\max} I(R_p, L_0, \varphi_0)$. With the leading velocity potential of the point source for the bubble, $I(R_p, L_0, \varphi_0)$ is both theoretically and numerically found to be $\propto -(R_p^3 \cos\varphi_0/L_0^2)$, following an inverse-square law of L_0 [16]. Thus, the normalized lift force reads

$$\langle F_z \rangle^* = \frac{\langle F_z \rangle}{\Delta p \pi R_p^2 \cos\varphi_0} \propto \frac{R_{b,\max}R_p}{L_0^2}, \tag{2}$$

as proven by the linear fitting for the cases of no bubble-particle contact, denoted by a solid line in Fig. 4(a).

With bubble-particle contact, the time-averaged lift force increases nonlinearly with increasing $R_{b,\max}R_p/L_0^2$ until $\langle F_z \rangle$ approaches a constant lift force of the same magnitude as $\Delta p \pi R_p^2 \cos\varphi_0$, guided by the dashed line in Fig. 4(a). This indicates that the lift force on a particle in a static liquid reaches its maximum when the time-averaged contact radius of the bubble with the particle equals R_p. Therefore, the evolution of the particle acceleration can be divided into two regimes: the unsteady liquid inertia dominated regime and the bubble contact dominated regime.

Assuming the particle motion in the liquid after bubble collapse is dominated by gravity, we obtain the relationship between the maximum vertical displacement of the particle and the initial parameters by $\Delta z_{\max} = v_{0,z}^2/(2g) = (\langle F_z \rangle \Delta T/m_p)^2(2g)^{-1}$. When the unsteady liquid inertia dominates, Eq. (2) leads to $(\Delta z_{\max}/\Delta z_0) \propto (R_{b,\max}/L_0)^4$, with a length scale

$$\Delta z_0 = \left(\frac{\rho}{\rho_p}\right)^2 \left(\frac{\Delta p}{\rho g}\right) \cos\varphi_0, \tag{3}$$

denoted by the solid line in Fig. 4(b). The bubble contact dominated regime has a limiting condition when the bubble is nucleated on the particle surface, i.e., $L_0/R_p \to 1$. With $\langle F_z \rangle^* \approx const$, $(\Delta z_{\max}/\Delta z_0)$ is proportional to $(R_{b,\max}/R_p)^2$ with a limiting value of $(R_{b,\max}/L_0)^2$; see the dashed line in Fig. 4(b).

In reality, the inevitable friction between the particle and the boundary exerts a torque, thus rotating the particle. However, the rotating motion plays a limited role in the particle's sudden acceleration, since friction works in the short period of time before the particle detaches from the substrate. Moreover, friction can be reduced by changing the materials of the particle and the boundary, e.g., into glass particles and polymethyl methacrylate (PMMA) substrates and the particle's rotation can be visualized by painting some patterns on the sphere. Our Supplemental Video shows the particle is accelerated without visible rotation [16].

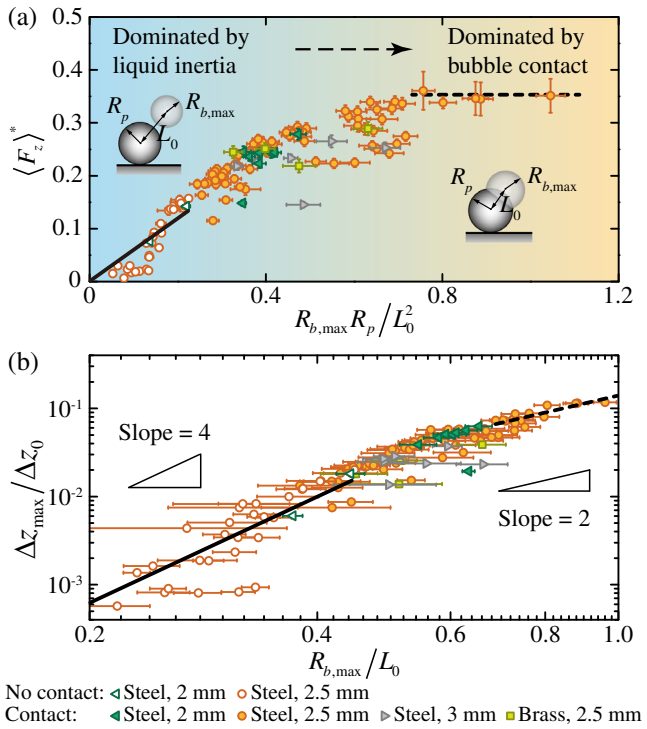

FIG. 4. Scaling laws controlling the particle acceleration. (a) Nondimensional time-averaged lift force estimated from experimental results versus $R_{b,\max}R_p/L_0^2$ for two dominant regimes. (b) Nondimensional maximum vertical displacement of the particle with Δz_0 defined by Eq. (3) versus $R_{b,\max}/L_0$. Solid lines indicate the scaling laws for the unsteady liquid inertia dominant regime and dashed lines for the bubble contact regime.

In conclusion, we find by experiments that, during the explosive growth of a laser-induced cavitation bubble of similar size, millimeter-sized spherical particles are suddenly accelerated like projectiles from a fixed rigid boundary. By estimating the time-averaged lift force on the particle during the bubble's growth and collapse, we propose two dominant regimes of the force, namely, the unsteady liquid inertia and the bubble-particle contact. For respective regimes, the fourth power and the square power laws are derived for the normalized maximum vertical displacement of the particle. The findings of this work may be helpful to the laser-assisted noninvasive manipulation of particles, e.g., on-demand collection of samples without mechanical contact from ground, and may be inspiring for the related situation of removing calculi and their fragments from tissues with reduced harm from ablation.

We gratefully acknowledge insightful discussions and helpful suggestions from H. A. Stone and C. Sun. We acknowledge financial support by the National Natural Science Foundation of China (NSFC, No. 11861131005, No. 52076120, and No. 52079066), the Deutsche Forschungsgemeinschaft (DFG, No. OH 75/3-1), the State Key Laboratory of Hydroscience and Engineering (2019-KY-04, sklhse-2019-E-02, and sklhse-2020-E-03), and the Creative Seed Fund of Shanxi Research Institute for Clean Energy, Tsinghua University.

*zhigang200@mail.tsinghua.edu.cn
†liushuhong@mail.tsinghua.edu.cn

[1] A. Karimi and J. L. Martin, Int. Met. Rev. **31**, 1 (1986).
[2] C. E. Brennen, *Cavitation and Bubble Dynamics* (Cambridge University Press, New York, 2014).
[3] D. Krefting, R. Mettin, and W. Lauterborn, Ultrason. Sonochem. **11**, 119 (2004).
[4] S. Zhu, F. H. Cocks, G. M. Preminger, and P. Zhong, Ultrasound Med. Biol. **28**, 661 (2002).
[5] C.-D. Ohl, M. Arora, R. Dijkink, V. Janve, and D. Lohse, Appl. Phys. Lett. **89**, 074102 (2006).
[6] G. L. Chahine, A. Kapahi, J.-K. Choi, and C.-T. Hsiao, Ultrason. Sonochem. **29**, 528 (2016).
[7] V. Minsier and J. Proost, Ultrason. Sonochem. **15**, 598 (2008).
[8] S. Poulain, G. Guenoun, S. Gart, W. Crowe, and S. Jung, Phys. Rev. Lett. **114**, 214501 (2015).
[9] S. Li, A.-M. Zhang, S. Wang, and R. Han, Phys. Fluids **30**, 082111 (2018).
[10] M. Arora, C.-D. Ohl, and K. A. Mørch, Phys. Rev. Lett. **92**, 174501 (2004).
[11] B. M. Borkent, M. Arora, C.-D. Ohl, N. de Jong, M. Versluis, D. Lohse, K. A. Mørch, E. Klaseboer, and B. C. Khoo, J. Fluid Mech. **610**, 157 (2008).
[12] S. Wu, Z. Zuo, H. A. Stone, and S. Liu, Phys. Rev. Lett. **119**, 084501 (2017).
[13] J. Zevnik and M. Dular, Ultrason. Sonochem. **69**, 105252 (2020).
[14] L. A. Teran, S. A. Rodríguez, S. Laín, and S. Jung, Phys. Fluids **30**, 123304 (2018).
[15] S. Wu, B. Li, Z. Zuo, and S. Liu, Phys. Rev. Fluids **6**, 093602 (2021).
[16] See Supplemental Material at http://link.aps.org/supplemental/10.1103/PhysRevLett.128.044501 for a document and videos. The document includes details on the superposition of velocity potentials of basic solutions and justification of the inverse-square law of the time-averaged lift force in the unsteady liquid inertia dominated regime. Supplemental videos show the cases A–D for the sudden accelerations of stainless steel particles from substrates made of stainless steel and a case for the sudden acceleration of a glass particle from a PMMA substrate.
[17] J. P. Best and J. R. Blake, J. Fluid Mech. **261**, 75 (1994).
[18] P. Weiss, Math. Proc. Cambridge Philos. Soc. **40**, 259 (1944).
[19] On the timescale of the bubble's collapse time ΔT_c, the Reynolds number of the flow is estimated as $\mathrm{Re} \sim O(\boldsymbol{U}\cdot\boldsymbol{\nabla U})/O(\nu\boldsymbol{\Delta U}) \sim (R_{b,\max}R_p)/(\nu\Delta T_c) \sim (R_p/\nu)\sqrt{[(p_\infty - p_v)/\rho]} \sim 2.5\times 10^4 \gg 1$, with $R_p = 2.5$ mm, $\nu = 10^{-6}$ m^2/s, $p_\infty = 101325$ Pa, $p_v = 2300$ Pa, and $\rho = 10^3$ kg/m^3. Therefore, viscous forces can be neglected.
[20] L. Rayleigh, Philos. Mag. **34**, 94 (1917).